

# Equilibrium Thermodynamics of Cell-Cell Adhesion Mediated by Multiple Ligand-Receptor Pairs

Daniel Coombs,\* Micah Dembo,<sup>†</sup> Carla Wofsy,<sup>‡</sup> and Byron Goldstein<sup>‡</sup>

\*Department of Mathematics, University of British Columbia, Vancouver, British Columbia V6T 1Z2, Canada; <sup>†</sup>Department of Bioengineering, Boston University, Boston, Massachusetts 02215 USA; and <sup>‡</sup>Theoretical Biology and Biophysics, MS K710, Los Alamos National Laboratory, Los Alamos, New Mexico 87545 USA

**ABSTRACT** In many situations, cell-cell adhesion is mediated by multiple ligand-receptor pairs. For example, the interaction between T cells and antigen-presenting cells of the immune system is mediated not only by T cell receptors and their ligands (peptide-major histocompatibility complex) but also by binding of intracellular adhesion molecules. Interestingly, these binding pairs have different resting lengths. Fluorescent labeling reveals segregation of the longer adhesion molecules from the shorter T cell receptors in this case. Here, we explore the thermal equilibrium of a general cell-cell interaction mediated by two ligand-receptor pairs to examine competition between the elasticity of the cell wall, nonspecific intercellular repulsion, and bond formation, leading to segregation of bonds of different lengths at equilibrium. We make detailed predictions concerning the relationship between physical properties of the membrane and ligand-receptor pairs and equilibrium pattern formation, and suggest experiments to refine our understanding of the system. We demonstrate our model by application to the T cell/antigen-presenting-cell system and outline applications to natural killer cell adhesion.

## INTRODUCTION

Adhesive pairs of ligands and receptors on cells can hold cell membranes in close apposition, and can act as signal transducers. This adhesion is selective and specific, in that a given cell will adhere tightly only to a small subset of others. In many situations, adhesion is mediated by a single pair of surface-bound macromolecules. However, experiments investigating T cell interactions with immobilized ligands (Grakoui et al., 1999) and T cell/antigen-presenting-cell (APC) interactions (for instance, Monks et al., 1998; Lee et al., 2002a; Moss et al., 2002; Freiberg et al., 2002; al et al., 2002) have sparked an interest in situations where two or more ligand-receptor pairs are responsible for binding. The key new feature introduced in this setting has been termed kinetic segregation (Davis and van der Merwe, 1996; Wild et al., 1999), where segregation of ligand-receptor pairs of different lengths is observed. The physical reason for this segregation is clear: if two ligand-receptor pairs of different lengths are in close proximity, the cell membrane must be locally deformed, with an associated energetic cost. In the absence of other effects, therefore, long and short ligand-receptor pairs will be segregated by length. This topological or topographical view of segregation was proposed for the T cell system in Shaw and Dustin (1997) and developed in Dustin and Shaw (1999) and Grakoui et al. (1999).

Theoretical studies of two-receptor systems and ligand-receptor segregation have so far been concerned with the T

cell system (Qi et al., 2001; Burroughs and Wülfing, 2002; Hori et al., 2002; Lee et al., 2002b; Weikl et al., 2002), and have examined the dynamics of cell membrane deformation and ligand binding during cell-cell and cell-lipid bilayer adhesion (further details are given below). In the analysis to follow, we examine the thermodynamic equilibrium of systems where adhesion is moderated by two binding pairs of molecules. We do not address the dynamic processes leading to the precise pattern of segregation of the ligand-receptor pairs. Our approach is to extend earlier theoretical studies of cell-cell adhesion mediated by a single ligand-receptor pair (Bell et al., 1984; Torney et al., 1986; Dembo and Bell, 1987).

A variety of effects may lead to the system not reaching equilibrium. These effects are often due to the fact that intercellular signaling mediated by cell-cell adhesion leads to alteration of membrane and receptor properties. The cytoplasmic domains of some receptors are known to have mechanical connections to the cell cytoskeleton (Burrige and Chrzanowska-Wodnicka, 1996; Jockusch et al., 1995). These connections mean that (even in the absence of signaling) the receptors are not freely mobile. Deviation from equilibrium behavior will be found if cytoskeletal rearrangements are a result of successful signal transduction (Forscher et al., 1992). For instance, in the T cell system, successful signal transduction leads to a reorganization of T cell receptors toward the region of close cell-cell apposition (Dustin et al., 1998; Wülfing and Davis, 1998; Krummel and Davis, 2002). In experiments performed in the presence of cytochalasin (an inhibitor of the cytoskeleton), kinetic segregation was unaffected, but further reorganization of the contact region did not occur (Grakoui et al., 1999).

Signaling may also alter the binding affinities of cell-surface receptors. For example, integrins such as LFA-1

*Submitted June 15, 2003, and accepted for publication November 10, 2003.*

Address reprint requests to Daniel Coombs, Dept. of Mathematics, University of British Columbia, Vancouver, British Columbia V6T 1Z2, Canada. Tel.: 604-822-2859; E-mail: coombs@math.ubc.ca.

© 2004 by the Biophysical Society

0006-3495/04/03/1408/16 \$2.00

(expressed on leukocytes) are usually inactive and thus prevent inappropriate binding. Binding of LFA-1 to its ligand (ICAM-1) is induced by signaling through other receptors and is believed to be modulated by clustering on the cell surface and molecular conformational changes (Hogg et al., 2002; Stewart and Hogg, 1996). In addition to modulation of binding affinities, signaling may lead to removal of cell-surface receptors. For example, T cell receptors (TCR) on resting T cells are believed to continuously cycle from the cytosol to the cell surface. On signaling, receptors may be down-regulated and degraded before recycling, resulting in a net loss of receptors from the surface (Liu et al., 2000). Further, peptide-MHC (the ligands of TCR) have been shown to be removed from APCs interacting with T cells, and internalized through TCR-mediated endocytosis (Huang et al., 1999).

Clearly, biological systems show considerable complexity that will not be amenable to equilibrium modeling. Nonetheless, careful study of a simplified system with well-defined physics will give insight into possible modes of asymptotic behavior. In studied T cell systems, the mature cell-cell contact is relatively stable for a long period (hours) after its formation. The importance of such phenomena as cytoskeletal rearrangement and receptor down-regulation can be gauged by the departure of the observed system from predicted equilibrium behavior. Further, equilibrium modeling is conceptually simple and computationally cheap: given a set of model parameters, whether or not cell-cell adhesion will result (and the equilibrium state, if it exists) can be determined in a matter of seconds.

Also, equilibrium cell-cell adhesion models are directly applicable to simplified experimental systems. For instance, it is possible to construct lipid vesicles bearing receptor species and observe vesicle-vesicle adhesion (studied theoretically by Bell and Torney (1985)). Extending to two ligand-receptor pairs would provide an exact experimental analog of the system we analyze here.

We present equilibrium models appropriate to two general settings: where two cells interact, and the simple extension to a system where a cell interacts with a flat, ligand-bearing membrane (such as the experimental system of Grakoui et al., 1999). Our strategy is to write down a function describing the change of free energy that occurs when two distant cells holding complementary ligands and receptors are brought together. This approach is identical to that taken for cell-cell adhesion mediated by a single kind of binding (Bell et al., 1984). Additional complexity is added by having more than one ligand-receptor pair, thus requiring inclusion of cell membrane bending terms. We present our model with two ligand-receptor pairs, but note that extensions to many pairs are within the model framework. The model includes a nonspecific repulsive interaction between nearby cell membranes, which the binding force must overcome if a region of close apposition is to form (Bongrand and Bell, 1984).

## Adhesion model

The change in free energy will be written as the sum of three distinct parts: i),  $\Delta F_b$ , free-energy changes associated with receptor binding; ii),  $\Delta F_r$ , free-energy changes due to nonspecific cell-cell repulsion; and iii),  $\Delta F_e$ , elastic energy terms arising from spatial variation in the membrane surface tension and curvature.

Fig. 1 illustrates our view of the cell-cell contact. Ligand binding occurs within a well-defined region of radius  $\rho_b$ . Because the two ligand-receptor pairs have different lengths, we do not expect this region to be flat.

We define the light-microscopic surface area of the ligand- and receptor-bearing cells to be  $A_L$  and  $A_R$ . The “resting” surface areas (before cell-cell contact) are denoted  $A_{LT}$  and  $A_{RT}$ . The true resting surface area is larger than this; the extra surface area is taken up by ruffles. In leukocytes, the excess of cell surface area contained in ruffles is known to be  $\sim 100\%$  (Schmid-Schönbein et al., 1980; Ting-Beall et al.,

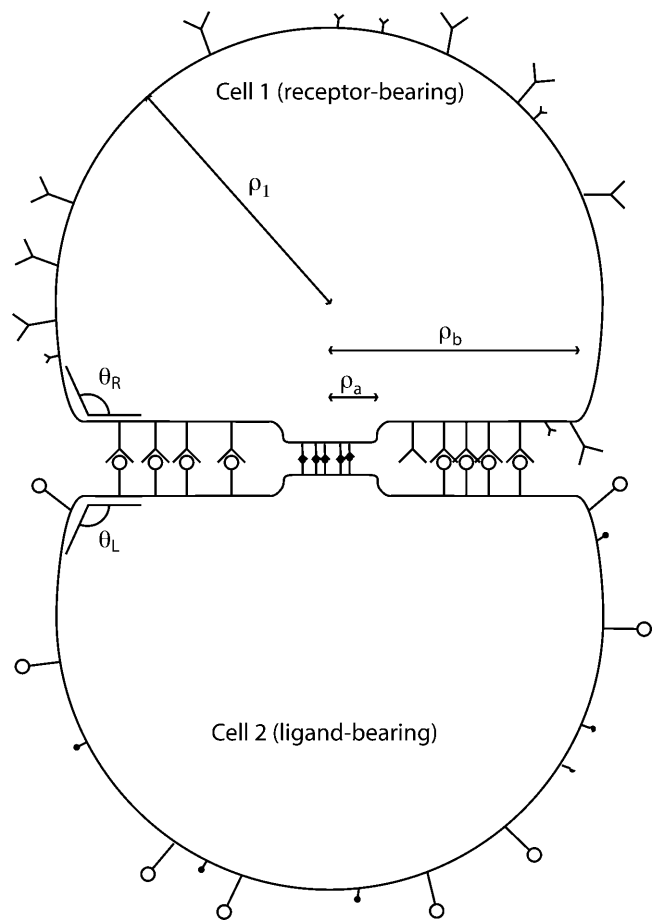


FIGURE 1 Schematic view of our model. Cell 1 bears two kinds of receptors, of different sizes, each of which may bind to its complementary ligand borne on cell 2. The geometry of cell 1 during cell-cell binding is also illustrated. The contact area is divided into two regions, of radius  $\rho_a$  and  $\rho_b$ , respectively. The cell forms a sliced sphere (frusta) shape, where the sphere has radius  $\rho_1$ . Also shown are the angles of contact for the two cells,  $\theta_R$  and  $\theta_L$ .

1993). The cell's visible surface area can increase up to the true surface area through stretching out of ruffles. Up to this limit, the surface tension is a measure of how difficult it is to stretch out ruffles. For simplicity, we assume that cell surface ruffles are smoothed out in the contact zone so that, in this region, the projected area is the same as the light-microscopic area and the surface tension is therefore assumed to be constant within the contact region. Hopefully, future experiments will indicate whether this is a valid approximation.

The energy change due to bond formation will depend on the membrane separation. We define the intermembrane separation at a point to be  $S(\vec{x})$ . We will denote the number of free (unbound) receptors on the first cell by  $R_1, R_2$ , and their concentrations at a point by  $r_1(\vec{x}), r_2(\vec{x})$ . Unbound receptors are assumed to freely diffuse. The numbers of each kind of free ligand on the second cell are  $L_1, L_2$ , and their concentrations at a point are  $l_1(\vec{x}), l_2(\vec{x})$ .  $L_i$  binds only  $R_i$ . We will assume that the bound ligand-receptor pairs are freely mobile in their respective cells. At equilibrium, free (unbound) ligands and receptors will be uniformly distributed over the entire cell surface (it is possible that longer receptors may be sterically excluded from regions of the adhesion region where the two cell membranes are closely apposed, but we do not consider this). The numbers and concentrations of bound complexes will be denoted by  $B_1, B_2, b_1(\vec{x})$  and  $b_2(\vec{x})$ . We further take the total numbers of receptors and ligands in the system to be fixed at  $R_{1T}, R_{2T}, L_{1T}$ , and  $L_{2T}$ . Therefore,  $R_{iT} = B_i + R_i$ , and  $L_{iT} = B_i + L_i$  ( $i = 1, 2$ ).

### Free-energy changes due to ligand binding

We divide  $\Delta F_b$ , the change in free energy due to ligand binding, into two parts,  $\Delta F_{b1}$  and  $\Delta F_{b2}$ , corresponding to the energy changes due to  $L_i + R_i \rightleftharpoons B_i$  for  $i = 1, 2$  respectively. Each of these then consists of two parts: loss of the chemical potential of a free receptor-ligand pair and gain of the chemical potential of a bound receptor-ligand pair. Noting that at equilibrium, free ligands and receptors are uniformly distributed over the cell surface, we have

$$l_i(\vec{x}) = l_i = \frac{L_i}{A_L}, \quad (1)$$

$$r_i(\vec{x}) = r_i = \frac{R_i}{A_R}. \quad (2)$$

We define the initial concentrations of ligands and receptors,  $\bar{l}_1 = L_{1T}/A_{LT}$ ,  $\bar{l}_2 = L_{2T}/A_{LT}$ ,  $\bar{r}_1 = R_{1T}/A_{RT}$  and  $\bar{r}_2 = R_{2T}/A_{RT}$ , and the chemical potential of free receptors  $\mu_{iR}$  and of free ligands  $\mu_{iL}$ . The loss of chemical potential of free receptors of the first type is now

$$\Delta F_{b1}^{(1)} = \int_{A_R} r_1 \mu_{iR}(r_1) d\vec{x} - R_{1T} \mu_{iR}(\bar{r}_1) \quad (3)$$

$$= R_1 \mu_{iR}(r_1) - R_{1T} \mu_{iR}(\bar{r}_1). \quad (4)$$

Similarly, the loss of chemical potential of free ligands of the first type is

$$\Delta F_{b1}^{(2)} = L_1 \mu_{iL}(l_1) - L_{1T} \mu_{iL}(\bar{l}_1). \quad (5)$$

We introduce the chemical potential of the bound state,  $\mu_{iB}$ , which is a function of the concentration of bonds and of the intermembrane separation. Then the free-energy change due to bond formation is

$$\Delta F_{b1}^{(3)} = \int_{A_c} b_1(\vec{x}) \mu_{iB}(b_1(\vec{x}), S(\vec{x})) d\vec{x}. \quad (6)$$

Following Bell et al. (1984), we will treat the bonds as linear springs of unstressed length  $\zeta_i$ :

$$\mu_{iB} = \mu_{iB}^0 + (1/2) \kappa_i (S(\vec{x}) - \zeta_i)^2, \quad (7)$$

where  $\kappa_i$  are bond spring constants. Adding these three parts gives the total free-energy change for the first kind of ligand-receptor interaction. The change due to the second kind of ligand-receptor interaction is identical, but with "2" replacing "1" in subscripts throughout. The chemical potentials are related to the affinities of their respective bonds at distance  $S$ ,  $K_i(S)$ , by the formula

$$K_i(S) = \exp\left(\frac{\mu_{iL} + \mu_{iR} - \mu_{iB} + k_B T}{k_B T}\right) \quad (8)$$

(for more details, see Bell et al., 1984).

### Nonspecific repulsion

Cells do not stick to each other in the absence of bridging bonds. We model this effect by introducing a weak nonspecific repulsion between the cell membranes. Therefore the cells will separate if the binding is not sufficiently strong. We represent this effect as an energy penalty for bringing the cell membranes into close apposition, writing

$$\Delta F_3 = \int \Gamma(S(\vec{x})) d\vec{x} = \int \frac{\gamma}{S} e^{-S/\tau} d\vec{x}, \quad (9)$$

where the integral is taken over the region in which bonds may form. The decreasing potential  $\Gamma(S)$  should diverge as  $S \rightarrow 0$ , and fundamentally should depend on two parameters: a characteristic decay length  $\tau$  and a strength  $\gamma$ . The exact form chosen is due to Bongrand and Bell (1984) (which also contains a discussion of the origin of the nonspecific repulsion). Qualitatively, this potential decays as the reciprocal of the separation distance out to a distance  $\tau$ , after which it decays more rapidly. Alternative models for the potential, including attractive forces, are easy to implement.

In the case of the T cell, certain of the long molecules that might be thought of as effectively part of the extracellular matrix (specifically, CD43 (Delon et al., 2002) and CD45 (Johnson et al., 2000)), are known to be excluded from the

mature cell-cell contact region. In modeling the nonspecific repulsion between the two cells, we use the form given above. We note, however, that steric exclusion or active transport of these and other long molecules from the contact region might lead to a decrease in the strength of the intercellular repulsion over time.

### Free-energy changes due to membrane deformations

The elastic energy of a cell membrane, which we picture as a uniform deformable elastic sheet, is the sum of bending and stretching components. A full description of the elastic energy associated with general deformations is certainly possible, but leads to considerable complexity. We shall develop an approximate theory that will capture the essential physics of the system. Specifically, we assume the following: 1), the change in bending energy of the membrane away from the contact region is negligible; 2), within the contact region, the membrane is approximately flat, except along boundaries between short-receptor rich regions and long-receptor rich regions. The local contribution to bending energy scales with the square of the local curvature. Therefore, the bending energy is concentrated along these lines, and we neglect bending energy elsewhere; 3), the surface tension is constant away from the contact region; and 4), the change in surface area of the cell is reasonably small in that the related change in energy is given by the surface tension of the “resting” cell times the change in surface area.

We can therefore write the change in free energy due to deformations of the two cells as the sum of a line energy and a surface stretching energy:

$$\Delta F_e = C_b \epsilon_b + (\delta A_L) \sigma_{LT} + (\delta A_R) \sigma_{RT}. \quad (10)$$

Here,  $C_b$  represents the total length of boundaries between short-receptor rich regions and long-receptor rich regions.  $\epsilon_b$  is the corresponding line tension. The calculation of  $\epsilon_b$  involves a simple application of elasticity theory and is detailed in the appendix.  $\delta A_L$  and  $\delta A_R$  are the changes in surface areas of the two cells, and  $\sigma_{LT}$  and  $\sigma_{RT}$  are the surface tensions of the two cells.  $\delta A_L$  and  $\delta A_R$  are found geometrically from the size of the contact area and the surface area of the noncontacting part of the cell.

### Geometrical simplifications

We are now in a position to minimize the total free energy of the system. However, significant simplifications can be made by making a few reasonable assumptions about the final pattern of receptor segregation. We first assume a separation of length scales between “long” and “short” bound pairs. Then, within the preceding framework, we see that given a certain number of bonds of each type, the free energy will be minimized when the total length of the boundaries

between long-bond rich and short-bond rich regions is at a minimum. Further, the terms  $(\delta A_L) \sigma_{LT}$  and  $(\delta A_R) \sigma_{RT}$  in the free energy penalize deviations of the whole contact region shape away from circular. This motivates our first geometric assumption, that the contact region is radially symmetric and has a “bull’s-eye” pattern of receptor-type boundaries. We also argue that the configuration of minimal free energy will have a single boundary between long and short bonds (this is observed in some experimental systems (Grakoui et al., 1999) but not others, for instance see Lee et al., 2002a). For an alternative approach to these questions, based on analysis of pattern formation in the contact region, see Hori et al., 2002. There, the intriguing possibility (supported by certain numerical and experimental data) of stable synaptic patterns of higher wavenumber (multiple regions of long and short segregated bonds) was suggested.

Motivated by these assumptions, we divide the contact region into two parts: an inner disk of radius  $\rho_a$  and a surrounding annulus  $\rho_a < \rho < \rho_b$ . We suppose that one type of bond will be predominantly clustered within  $\rho_a$  and the other in the annulus out to  $\rho_b$ . The model geometry is shown in Fig. 1. We call the numbers and concentrations of bonds of types 1 and 2, in regions  $a$  and  $b$ ,  $B_{1a}$ ,  $B_{2a}$ ,  $B_{1b}$ ,  $B_{2b}$ ,  $b_{1a}$ ,  $b_{2a}$ ,  $b_{1b}$ , and  $b_{2b}$ , respectively. We further assume that the width of the interface at  $r = \rho_a$  is small compared to  $\rho_b$  and that the membrane separations in the two regions, which we will call  $S_a$  and  $S_b$ , are spatially uniform and selected at equilibrium exclusively by the balance between nonspecific repulsion forces and binding forces.

### Complete free energy

Putting the terms together in the simplified geometry, the free energy is now the sum of the following:

#### Energy change due to formation of type 1 (short) bonds

$$\begin{aligned} \Delta F_{b1} = & R_1 \mu_{1R}(r_1) - R_{1T} \mu_{1R}(\bar{r}_1) + L_1 \mu_{1L}(r_1) - L_{1T} \mu_{1L}(\bar{l}_1) \\ & + \pi \rho_a^2 b_{1a} \mu_{1B}(b_{1a}, S_a) + \pi(\rho_b^2 - \rho_a^2) b_{1b} \mu_{1B}(b_{1b}, S_b). \end{aligned} \quad (11)$$

#### Energy change due to formation of type 2 (long) bonds

$$\begin{aligned} \Delta F_{b2} = & R_2 \mu_{2R}(r_2) - R_{2T} \mu_{2R}(\bar{r}_2) + L_2 \mu_{2L}(r_2) - L_{2T} \mu_{2L}(\bar{l}_2) \\ & + \pi \rho_a^2 b_{2a} \mu_{2B}(b_{2a}, S_a) + \pi(\rho_b^2 - \rho_a^2) b_{2b} \mu_{2B}(b_{2b}, S_b). \end{aligned} \quad (12)$$

#### Energy change due to nonspecific repulsion between the cells

$$\Delta F_3 = \pi \rho_a^2 \Gamma(S_a) + \pi(\rho_b^2 - \rho_a^2) \Gamma(S_b). \quad (13)$$

### Energy change due to elasticity of the cell membranes

$$\Delta F_e = 2\pi\rho_a \epsilon_b + (\delta A_L)\sigma_{LT} + (\delta A_R)\sigma_{RT}. \quad (14)$$

The total free energy is a function of six variables:  $\rho_a$ ,  $\rho_b$ ,  $S_a$ ,  $S_b$ ,  $B_1$ , and  $B_2$ . From these variables, we can calculate the different concentrations of bound states ( $b_{1a}$ ,  $b_{2a}$ ,  $b_{1b}$ , and  $b_{2b}$ ) in the two regions. At equilibrium, the concentrations of free ligands and receptors (of each type) are equal. Therefore, by the law of mass action, the concentration of (for example) bonds of the first type in the inner and outer regions are  $b_{1a} = K_1(S_a)r_1l_1$  and  $b_{1b} = K_1(S_b)r_1l_1$ , respectively. The fraction of bonds of type 1 in the inner region is therefore

$$\frac{B_{1a}}{B_1} = \frac{\pi\rho_a^2 K_1(S_a)}{\pi\rho_a^2 K_1(S_a) + \pi(\rho_b^2 - \rho_a^2)K_1(S_b)}. \quad (15)$$

Equivalently, using Eq. 8 to express the equilibrium constants, we can write the number of such bonds in the inner region as

$$B_{1a} = B_1 \left( \pi\rho_a^2 e^{-\frac{\kappa_1(S_a - \zeta_1)^2}{k_B T}} \right) / \left( \pi\rho_a^2 e^{-\frac{\kappa_1(S_a - \zeta_1)^2}{k_B T}} + \pi(\rho_b^2 - \rho_a^2) e^{-\frac{\kappa_1(S_b - \zeta_1)^2}{k_B T}} \right). \quad (16)$$

Similar expressions are used to find  $B_{1b}$ ,  $B_{2a}$ , and  $B_{2b}$ . This expression also shows the degree of segregation of the bond types between regions of thickness  $S_a$  and  $S_b$ . For example, for the T cell system, the two bond lengths are 15 nm and 42 nm, with the bond elasticities  $\sim 0.1$  dyn/cm (Table 1). Using these numbers and taking  $S_a = 15$  nm and  $S_b = 42$  nm, we can estimate  $K_1(S_b) = (1.2 \times 10^{-8})K_1(S_a)$ . Equation 15 indicates that, for  $\rho_a$  and  $\rho_b$  both on the micron scale, we will have essentially perfect segregation of long and short bonds into different such regions. Conditions for segregation in dynamic models of synapse formation were considered by Burroughs and Wülfing (2002) and Hori et al. (2002).

All that remains to be done is to link the deformed geometry of the cell to  $\rho_a$  and  $\rho_b$ . Let the original radius of the cell be  $\rho_0$  with original volume  $V_0 = (4/3)\pi\rho_0^3$ . The volume of the deformed sphere (frustum) illustrated in the upper half of Fig. 1 is

$$V_1 = \frac{\pi}{3}\rho_1^2 \left( 2 \left( 1 + \frac{h}{\rho_1} \right) \rho_1 + \rho_b^2 h \right), \quad (17)$$

where  $h = \sqrt{\rho_1^2 - \rho_b^2}$ . Conservation of volume for the cell means that  $\rho_1$  satisfies  $V_1 = V_0$ . There is a single real solution for  $\rho_1$  as a function of  $\rho_b$  and  $\rho_0$ . To lowest contributing order,  $\rho_1/\rho_0 = 1 + (1/16)(\rho_b/\rho_0)^4$ . The surface area of the deformed cell is therefore

$$2\pi\rho_1(h + \rho_1) + \pi\rho_b^2. \quad (18)$$

The outer surface tension is fixed. To find the surface tension within the contact area, we use the angles of contact (see Fig. 1)

$$\theta_L = \cos^{-1} \sqrt{1 - \frac{4\pi\rho_b^2}{A_{LT}}}, \quad \theta_R = \cos^{-1} \sqrt{1 - \frac{4\pi\rho_b^2}{A_{RT}}} \quad (19)$$

and the relations  $\sigma_L = \sigma_{LT} \cos \theta_L$  and  $\sigma_R = \sigma_{RT} \cos \theta_R$ .

The system is subject to the constraints  $0 \leq B_1 \leq \min(R_{1T}, L_{1T})$ ,  $0 \leq B_2 \leq \min(R_{2T}, L_{2T})$ ,  $0 \leq \rho_a \leq \rho_b < \rho_{\max}$ ,  $0 < S_a$ ,  $0 < S_b$ , where  $\rho_{\max}$  is taken to be the diameter of the resting cell.

### Generalization to supported bilayer experiments

The preceding model can be modified to approximate the free-energy change due to binding of a cell to a receptor-bearing, flat, supported bilayer. The supported bilayer is assumed to be fixed, so it has no bending or stretching energy. A derivation of the energy density of interfaces between short and long bonds for this case is presented in the appendix. The free energies  $\Delta F_{b1}$ ,  $\Delta F_{b2}$  and  $\Delta F_3$  are as given above, but we now have

$$\Delta F_e = 2\pi\rho_a \epsilon_b + (\delta A)\sigma_T, \quad (20)$$

where  $\delta A$  and  $\sigma_T$  are properties of the cell alone.

### Reversed patterns

The general view of this kind of cell-cell adhesion from T cell experiments is that the longer bonds will surround the short bonds. However, it is feasible that under some circumstances, an equilibrium state might show a reversed pattern. It should be noted that there is nothing in the model so far to exclude this possibility. For example, consider a situation where two cells have formed a synapse where the long bonds surround the short bonds. Then, gradually increase the available number of short ligands and receptors. As this is done, the central region expands due to the trade-off between the change in free energy due to the additional short bonds and the energetic cost of the lengthier interface. At some point, reversing the synapse pattern will make the length of the interface shorter without altering the number of

**TABLE 1 Comparison of previously published parameter estimates for T cell adhesion**

Parameter	Qi et al. (2001)	Burroughs and Wülfing (2002)
$K_1$	$10^{-9}$ cm <sup>2</sup> and $5 \times 10^{-7}$ cm <sup>2</sup>	$2 \times 10^{-9}$ cm <sup>2</sup>
$K_2$	$3.3 \times 10^{-8}$ cm <sup>2</sup>	$2 \times 10^{-9}$ cm <sup>2</sup>
$\zeta_1, \zeta_2$	15 nm, 42 nm	14 nm, 41 nm
$\kappa_1, \kappa_2$	$2 \times 10^{-4}$ dyne/cm	$4 \times 10^{-2}$ dyne/cm
$\beta_R$	$1.6 \times 10^{-11}$ erg	$5 \times 10^{-13}$ erg
$\sigma_{RT}$	$3.1 \times 10^{-3}$ dyne/cm	$2.4 \times 10^{-2}$ dyne/cm

bonds (of course, this is slightly too simple as the radius of the outer region will also generally be changing).

### Qualitative behavior of model

We illustrate the model by looking at contact formation between two identical cells as a function of the strength of intercellular repulsion. We suppose the cells are geometrically identical with a resting surface area of  $5 \times 10^{-6} \text{ cm}^2$  and that they present  $10^4$  of each kind of receptor and ligand, with affinity  $10^{-8} \text{ cm}^2$ . Both bonds have a spring constant of  $0.1 \text{ dyn/cm}$ , and have lengths  $10 \text{ nm}$  and  $40 \text{ nm}$ . The length scale of the intercellular repulsion is taken to be shorter than the shorter bond,  $\tau = 5 \text{ nm}$ . Finally, the bending moduli of the cells are taken to be  $5 \times 10^{-13} \text{ erg}$  and the surface tensions are taken to be  $0.1 \text{ dyn/cm}$ .

Results are presented in Fig. 2. First, the fraction of binding of “long” and “short” bonds is shown (note, we find essentially complete segregation of the long and short bonds between the two regions). As the intercellular repulsion increases, the number of short bonds formed decreases continuously to zero. We also indicate the radii of the inner and outer regions and the intercellular separation in the inner region. The cell-cell separation gap in each zone depends on the balance between repulsive forces and densities of different species. Because the repulsive potential between the cells drops off rapidly, the separation is essentially constant and equal to  $40 \text{ nm}$  in the outer region. As the repulsion strength increases, the separation in the central region increases and the number of bonds there decreases. As the number of bonds decreases, so does the inner radius  $r_a$ . Eventually, as  $\gamma$  increases, the energy

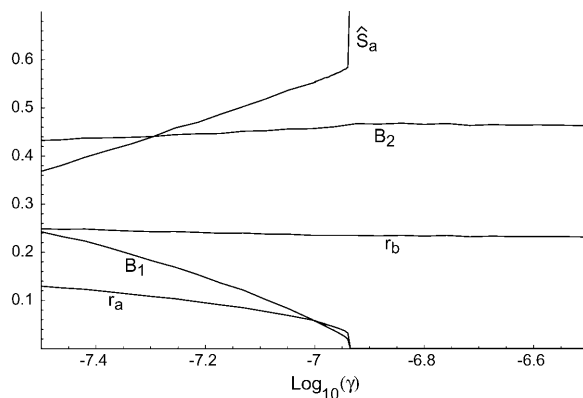


FIGURE 2 Illustration of the model. The parameter  $\gamma$ , which determines the strength of cell-cell repulsion, is varied. Other parameters are given in the text. We plot the number of short ( $B_1$ ) and long ( $B_2$ ) bound receptors as a fraction of their total amounts. The radii  $r_a$ ,  $r_b$ , are plotted as a fraction of the resting cell radius (the same for both cells in this case). The separation of the two membranes within the inner (short) contact area is shown by  $\hat{S}_a = (S_a - \zeta_1)/\zeta_1$ , where  $\zeta_1$  is the unstretched length of the short bond. When  $\hat{S}_a = 0$ , the bond is unstretched.  $\gamma$  is the strength of the intercellular repulsion (Eq. 9).

decrease due to binding is less than the elastic cost of sustaining the interface. The number of long bonds increases slightly as the interface gets small, as the space available for long bonds increases. The radius of the whole contact area,  $r_b$ , is set in this case by the competition between the energy of formation of long bonds and the energy penalty for deformation of the cells to include a contact area (set by the surface tension) and does not change much over the range of  $\gamma$  considered.

### CASE STUDY: T CELL/ANTIGEN-PRESENTING-CELL ADHESION

We demonstrate our approach by application to the equilibrium state of a T cell/APC contact. We begin by discussing some biological background and previous modeling efforts.

#### Biological background

T cell activation is mediated by the formation of transient bonds between TCR and peptide fragments (called antigens, if derived from a foreign organism) presented on the surface of an APC. If the presented peptides are recognized by the TCR, a stable region of close cell-cell contact forms and is maintained for several hours. If they are not recognized, the T cell will move on to investigate other cells within a few minutes. The region of close apposition is termed the immunological synapse or supramolecular activation complex, and its formation and maintenance are believed to be important for full T cell signal transduction (Monks et al., 1998; Krummel and Davis, 2002).

Typically, a mature T cell expresses  $\sim 30,000$  identical TCR, which bind to a small class of presented peptides. The APC will usually present a spectrum of peptides, most of which are self-peptides that are not by themselves recognized by T cells (but which may have a costimulatory effect (Wülfing et al., 2002)). The peptides are displayed on the cell surface bound to an MHC (major histocompatibility complex) molecule. Presented peptide-MHC (pMHC) that lead to T cell activation are termed agonists. The interaction between the two cells is not mediated solely by the TCR-peptide-MHC interaction. Rather, several other ligand-receptor pairs act to stabilize the synapse region, and some have costimulatory or other important signaling effects. Importantly, these secondary interactions are not thought to be antigen-specific, in that they occur equally between any T cell/APC pair, independent of the peptides presented. An important secondary interaction is that between the adhesion molecules LFA-1 (presented on the T cell) and ICAM-1 (on the APC). From our perspective, the key feature is that this binding pair of molecules are considerably longer ( $\sim 42 \text{ nm}$ ) than the TCR-peptide-MHC pair ( $\sim 14 \text{ nm}$ ). Therefore, coexistence of the two binding pairs in a spatially localized region requires local bending of the cell membranes, and one

observes separation of the two in experiments as described below.

In many experiments, different teams have investigated the spatial patterns formed due to segregation of the short and long bonds in this system. One particularly clear experiment (Grakoui et al., 1999) replaces the APC with a planar bilayer, to which is bound only peptide-MHC and ICAM-1. These molecules are fluorescently labeled and the formation of patterns is observed when a T cell reaches the bilayer, recognizes the presented peptide-MHC, and forms a long-lasting attachment. Further, regions of closer apposition between the cell and the bilayer can be observed, and these correlate well with high concentrations of peptide-MHC (the shorter of the two binding molecules). The dynamics of patterning are as one might expect: as the T cell approaches the planar bilayer from above, the first contacts made are between the longer (LFA-1/ICAM-1) binding pairs. Fluctuations locally bring the TCR-peptide-MHC pairs into contact, forming bonds with relatively high affinity. The formation of these bonds leads to regions of close membrane-bilayer apposition, and thus steep (energetically unfavorable) gradients in the position of the cell membrane. After 3–5 min, an approximately disk-shaped region of shorter bonds is found toward the center of the nascent synapse, surrounded by an approximate annulus of longer bonds. This bull's-eye configuration then persists for hours. Thermodynamically, it can be argued that in the absence of thermal fluctuations, circular symmetry would minimize the line energy due to bending of the membrane at the interface between long and short bonds, and the configuration of the bull's-eye pattern permits the cell to be closer to its preferred, approximately spherical shape. However, much experimental work (Grakoui et al., 1999; Moss et al., 2002) indicates that cytoskeletal forces also play a role, acting directly on the TCR and relocating them toward a focal point.

The physiological importance of forming a stable synapse in cell-cell contacts is unclear. It is observed that many important cytosolic signaling molecules relocate to the synapse region after stimulation of the cell by recognized pMHC, although further investigations have also shown the exclusion of other signaling molecules (Freiberg et al., 2002; van der Merwe, 2002; Krummel and Davis, 2002). The synapse may act as a focus for the release of soluble cytokines from the T cell, destined to bind receptors on the APC (Kupfer et al., 1991, 1994; van der Merwe and Davis, 2002). Several groups have shown that synapse formation is not necessary for some aspects of signaling to occur (Lee et al., 2002a). Results vary significantly among different cell types.

One final detail that may be important from the point of view of this article is the existence of other pairs of adhesion molecules that may aggregate in the synapse. One such pair is CD2-CD48/58, with bond length similar to that of TCR-pMHC. Experimental evidence suggests that this interaction may be important in stabilizing the cell membranes in close

proximity (Dustin et al., 1997). Also, weakly binding (non-agonist) pMHC groups may be regarded as nonantigen-specific short bonds. As we show below, TCR-pMHC at physiological densities may not be sufficient to produce the bull's-eye pattern of the immunological synapse. However, if enough additional short ligand-receptor pairs are present, our conclusions are altered.

## Modeling of synapse formation

The dynamics of synapse formation have been studied theoretically, although many questions remain. Two groups adopted similar modeling strategies to produce a system of partial differential equations describing the spatio-temporal evolution of the four unbound species and two bound species in the system, and of the shape of the cell membrane at the interface (Qi et al., 2001; Lee et al., 2002b; Hori et al., 2002; Burroughs and Wülfing, 2002). In both cases, the equations permit two-dimensional diffusion of all species in the plane of the synapse, with the rates of bond formation at a point assumed to depend on the membrane separation there. Elastic bending and stretching deformations of the T cell membrane are included within the models. Both models predicted segregation of bonds of different lengths due to the significant free-energy cost of bond stretching or compression. Burroughs and Wülfing (2002) further concluded that cytoskeletal forces (modeled by selective advection of TCR toward the synapse center) are necessary for the central aggregation of TCR and surrounding ring of LFA-1/ICAM-1. Differences in parameter estimates and details of the modeling make it difficult to make a detailed comparison of the conclusions drawn from the models.

## RESULTS

We implemented the presented equilibrium model with one simplification: we assumed total segregation of the longer and shorter bound ligand-receptor pairs. This is justified by the experimental observation that kinetic segregation is strict in this system, and by theoretical considerations (Burroughs and Wülfing, 2002). The energy functional (augmented with steep penalties outside the feasible region) was minimized using Powell's derivative-free method with multiple restarts (Press et al., 1988). The minimizers found were verified for test cases using the simplex method.

The number of agonist pMHC presented to the T cell may be as few as three or four for early cell signaling events to occur (Moss et al., 2002). There is also evidence that the potency of a given pMHC is determined by the half-life with which it binds TCR (Vallitutti et al., 1996; Kalergis et al., 2001; Coombs et al., 2002). Our model can only distinguish between pMHC on the basis of affinity for TCR. Rather than modeling each of the group of identical presented pMHC separately, we consider a single population that may be thought of as an effective average of the presented species

(and therefore may be larger in number than the number of presented agonists). Recent experiments provide some evidence that the effectiveness of a pMHC in triggering T cell activation is correlated with binding affinity (Holler and Kranz, 2003). One further consideration is that the short bonds may be considered not only to model TCR-pMHC, but also CD2-CD48/58 interactions. Therefore, it is of interest to see what happens when the number of short ligands/receptors exceeds the number of TCR and pMHC available.

### Adhesion mediated by LFA-1/ICAM-1 interactions alone

We begin by applying our model to the question of when cell-cell adhesion will occur in the absence of specific TCR-pMHC binding. Within our model, set  $B_1 = \rho_a = 0$ . Note that we include effects of surface tension, and therefore, our model does not reduce to that of Bell et al. (1984). As discussed in the introduction, the affinity of the LFA-1/ICAM-1 bond changes after stimulation of the T cell and the spatial distribution of LFA-1 may change. Within our model, we examine the effects of changing affinity and concentration of LFA-1. All other parameters are given in Table 2 ( $\gamma = 10^{-6}$  dyn,  $\tau = 10$  nm). Fig. 3 *a* is a contour plot of the level of binding of ICAM-1 as a function of the total number of LFA-1 on the T cell ( $R_{2T}$ ) and their binding affinity ( $K_2$ ). As

**TABLE 2** Typical parameters for T cell-APC system

Description	Symbol	Estimate
Number of TCR and pMHC	$R_1, L_1$	$3 \times 10^4, 100-1000$
Number of LFA-1 and ICAM-1	$R_2, L_2$	$2-3 \times 10^5, 1 \times 10^5$
Affinity of TCR-pMHC bond	$K_1$	$10^{-11} \text{ cm}^2-10^{-9} \text{ cm}^2$
Affinity of ICAM-1/LFA-1 bond	$K_2$	$10^{-9} \text{ cm}^2$
Unstrained lengths of bonds	$\zeta_1, \zeta_2$	$1.4 \times 10^{-6} \text{ cm}, 4.1 \times 10^{-6} \text{ cm}$
Spring constants for bonds	$\kappa_1, \kappa_2$	$0.1 \text{ dyn/cm}$
Intercellular repulsion strength; length scale	$\gamma, \tau$	$10^{-7}-10^{-6} \text{ dyn}, 10^{-7}-10^{-6} \text{ cm}$
Resting surface areas of cells	$A_{RT}, A_{LT}$	$5 \times 10^{-6} \text{ cm}^2$
Bending moduli of cells	$\beta_L, \beta_R$	$5 \times 10^{-13} \text{ erg}$
Resting surface tensions of cells	$\sigma_{LT}, \sigma_{RT}$	$0.1 \text{ dyn/cm}$

See Appendix 2 for references.

would be expected, the number of bound LFA-1 increases with both variables. If these parameters are sufficiently small, no binding occurs. In Fig. 3 *b*, we show the radius of the circular contact region. Fig. 3, *c* and *d*, show how the results change if the surface tensions  $\sigma_{RT}, \sigma_{LT}$  are increased by a factor of 10. As we would predict, increasing the surface tension makes the cell-surface stretching necessary for formation of a large contact region more energetically costly, and therefore the size of the contact region and number of bonds formed becomes smaller.

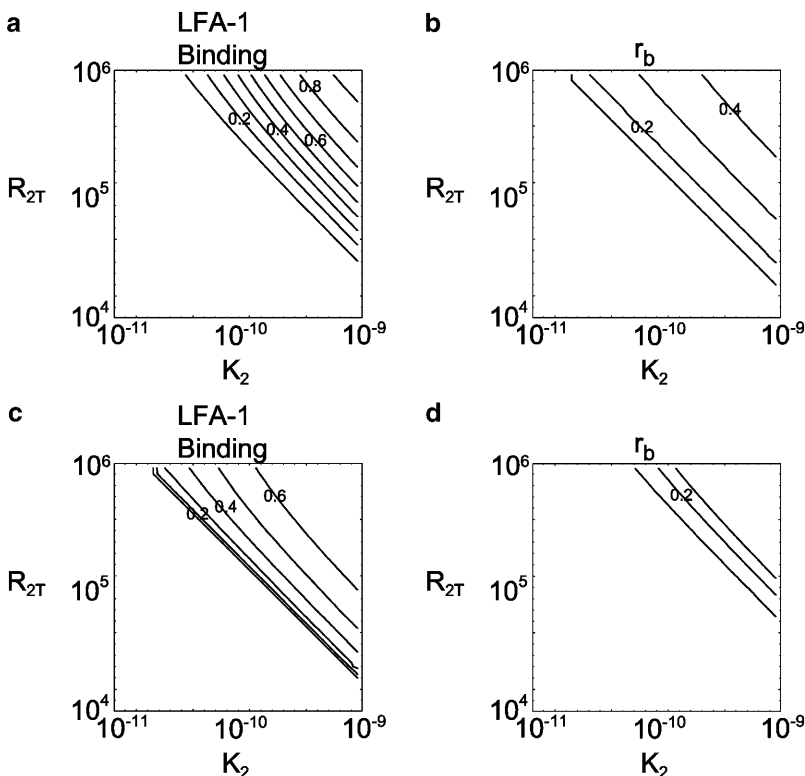


**FIGURE 3** Adhesion moderated purely by LFA-1/ICAM-1 binding. (*a*) The contours of the fraction of LFA-1 that are bound in equilibrium as a function of LFA-1 number ( $R_{2T}$ ) and the affinity of their interaction with ICAM-1 ( $K_2$ ). Contour interval is 0.1. (*b*) The radius of the contact region, as a fraction of the resting radius of the cell ( $6.3 \mu\text{m}$ ). Contour interval is 0.1. *c* and *d* repeat this but with the cell surface tensions  $\sigma_{RT}, \sigma_{LT}$  increased from 0.1 to 1 dyn/cm.

## Formation of immunological synapse

We now look at situations where both ligand-receptor pairs are present. We begin by comparing equilibrium behavior with previous dynamic models of synapse formation on supported bilayers and between cells.

### Comparison with Qi et al. (2001) and Lee et al. (2002b)

This modeling work describes the spatio-temporal evolution of molecular patterns in the immunological synapse between a T cell and a supported bilayer bearing defined pMHC and ICAM-1. We note that the system of equations used includes terms that prevent an equilibrium state from being reached. These terms model advection of TCR due to cytoskeletal motion and internalization of TCR after binding. If these effects were removed from the model, we would expect a stable equilibrium to be reached eventually. Further, this model does not include a nonspecific repulsion between the T cell and the supported bilayer.

Lee et al. (2002b) show a phase diagram indicating when a stable, “bull’s-eye” synaptic pattern is reached within their model, as a function of the kinetic parameters  $k_{\text{on}}$ ,  $k_{\text{off}}$  for the TCR-pMHC interaction. A range of dissociation constants between  $K_d \simeq 30\mu\text{m}^{-2}$  and  $K_d \simeq 6\mu\text{m}^{-2}$  are shown to possibly lead to a stable synapse formation (in fact, certain combinations of the kinetic parameters within this range do not lead to stable synapse formation; this is presumably due to internalization of TCR). We reproduce this phase diagram over values of  $K_1$  using different numbers of pMHC ( $L_{1T}$ ) in Fig. 4, and using the parameters given in Table 1. We used  $\gamma = 0$  (no intercellular repulsion), and  $R_{1T} = 10^5$ ,  $R_{2T} = L_{2T} = 2 \times 10^4$  (Lee et al., 2002c). Note that their model uses an initial uniform concentration of free pMHC on a supported

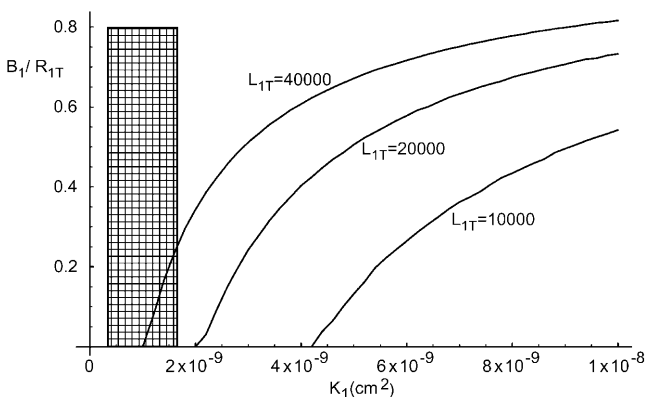


FIGURE 4 Formation of short bonds (TCR-pMHC) as a function of their affinity in an analogous simulation to that of Lee et al. (2002b).  $B_1/R_{1T}$  is the fraction of TCR that are bound to pMHC.  $K_1$  is the equilibrium constant for this reaction. The shaded area indicates the range of affinities for which they predict a quasi-equilibrium synapse (see text for explanation).

bilayer. Our cell-cell model considers two cells with a defined number of pMHC available. Because, in their model, pMHC may diffuse into the synapse from the surrounding area, for a reasonable comparison, we must consider different levels of short ligands (pMHC). The shaded region of Fig. 4 gives the range of affinities over which Lee et al. (2002b) predict synapse formation. Our conclusions are somewhat different. We do not predict a preferred range of affinities for the existence of a stable synapse configuration. Rather, for a given number of pMHC available, we find a minimum value for the affinity above which a stable synapse exists. The differences in our results must be attributed to advection and down-regulation of TCR in their dynamic model.

### Comparison with Burroughs and Wülfing (2002)

A major result of this modeling effort was that central aggregation of TCR does not occur in the absence of directed motion of TCR toward the center of the synapse region. We examine this statement in the context of our model. In the absence of directed motion, the model presented by Burroughs and Wülfing (2002) should come to equilibrium eventually. (The time to reach equilibrium may be long, however.) The main differences between our models lie in the nonspecific interactions between the two membranes and in the boundary conditions. The functional form they use for the nonspecific interactions is

$$\Gamma(S) = \frac{w}{2}(S - S_0)^2, \quad (21)$$

with  $w = 5 \times 10^7$  dyne  $\text{cm}^{-3}$  and  $S_0 = 27.5$  nm (midway between the lengths of the long and short bonds). Within this model, in the absence of binding, the two cell membranes are held at separation  $S_0$ . In our picture of cell-cell adhesion, this effective adhesive force (Eq. 21) will balance with the surface tension forces due to deformation of the cells to give a well-defined area of close contact. But in the simulations of Burroughs and Wülfing, only this region of close contact is studied, with the condition that the membrane separation is flat ( $dS/dr = 0$ ) at the boundary. In contrast, our model incorporates the other parts of the cell membrane.

We present results using Eq. 21 for the nonspecific interaction along with the parameters given in Table 1. We present a phase plane showing different equilibrium states as a function of the numbers of available short (pMHC and CD48) ligands on the APCs and long receptors on the T cell (LFA-1) (denoted by  $L_{1T}$  and  $R_{2T}$ , respectively). We take the number of cognate short receptors (CD2 and TCR) to be  $R_{1T} = 5 \times 10^4$ , corresponding to a density of  $100/\mu\text{m}^2$ , and the number of ICAM-1 to be  $9 \times 10^4$ , corresponding to  $180/\mu\text{m}^2$ . Five behaviors are possible: no cell-cell adhesion, adhesion mediated entirely by TCR-pMHC bonds, adhesion moderated entirely by LFA-1/ICAM-1 bonds, and coexistence in two states: “normal” (short bonds inside) and “reversed” (long bonds inside). Fig. 5 a shows our results.

We do find a region of the parameter space (region IV) in which an “immunological synapse” exists at equilibrium. This result must be due to our handling the boundary conditions and noncontacting regions of the cells differently than Burroughs and Wülfing. We also find a reversed immunological synapse configuration (region V) when more long (LFA-1/ICAM-1) bonds form than short bonds. Note the symmetry of the parameters: because  $K_1 = K_2$ ,  $\kappa_1 = \kappa_2$ , and  $S_0 = (\zeta_1 + \zeta_2)/2$ , initial formation of either bond is energetically equivalent. This observation explains the existence of the direct transition between regions II and III

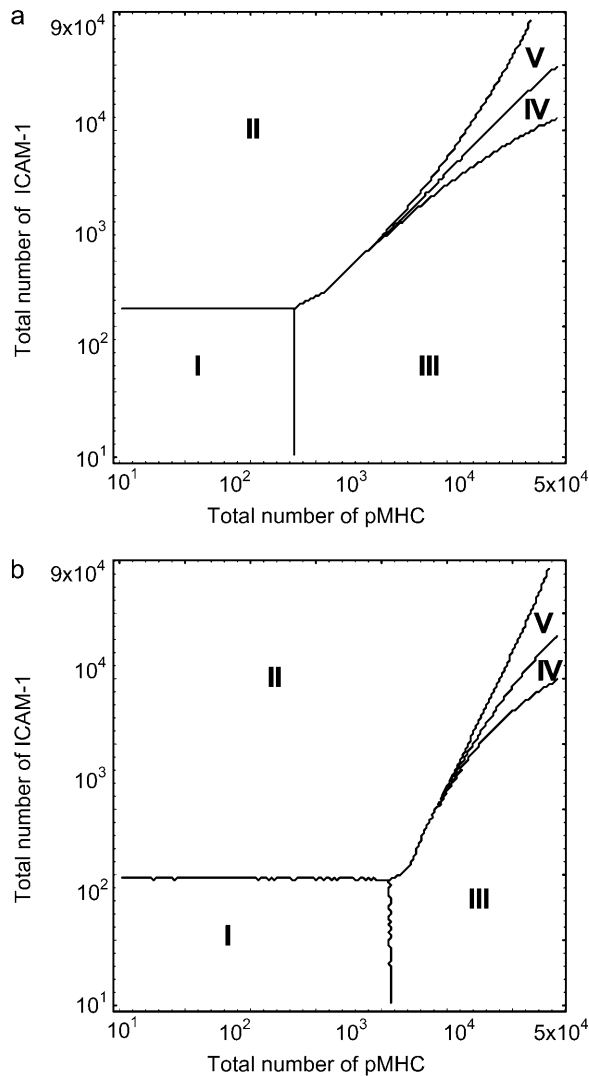


FIGURE 5 Phase diagrams of binding of T cells to antigen-presenting cells in the general description of Burroughs and Wülfing (2002): *a* shows results using the intercellular potential of Burroughs and Wülfing (2002) (Eq. 21), whereas *b* uses our potential (Eq. 9). Key: region I, no binding; II, binding solely of ICAM-1/LFA-1 (long bonds); III, binding solely of TCR-pMHC (short bonds); IV, both species bind with TCR-pMHC bonds in the center (immunological synapse); and V, both species bind with ICAM-1/LFA-1 bonds in the center (reversed synapse).

as more pMHC are made available. The existence of a transition between short and long bonds is only favored in our model if it allows enough extra bonds to be formed to offset the energy cost of the transition. In Fig. 5 *b*, we show how our predictions change if we use the function (Eq. 9) for the intercellular interaction potential, with range  $\tau = 5$  nm and strength  $\gamma = 10^{-7}$  dyn. In particular, the symmetry of the phase plane is broken because the shorter bonds feel the effect of the intercellular repulsion far more strongly than the long bonds.

### Cell-cell adhesion modulated by affinity and ligand/receptor concentration

Here we examine how equilibrium T cell/APC adhesion is affected by changes in binding affinity and cell surface concentration of LFA-1. We use the parameters given in Table 2 as a starting point. Results are presented in Fig. 6. Part *a* shows the effect of increasing the availability of short ligands (pMHC) in the absence of any intercellular repulsion ( $\gamma = 0$ ). For low values of  $K_2$  and  $L_{2T}$ , the all-long configuration is replaced by an all-short configuration. As  $K_2$  and  $L_{2T}$  increase, a classic synapse configuration becomes stable, followed by a “reversed synapse”. Part *b* shows the effect of including a small intercellular repulsion in the model ( $\gamma = 10^{-7}$  dyn,  $\tau = 5$  nm). This makes short bonds less energetically favorable without changing the properties of the long bonds very much. Therefore, the phase plane is shifted to lower  $K_2$ ,  $L_{2T}$ . Part *c* shows the effect of an increase in the surface tensions of the two cells from 0.05 dyn/cm to 0.25 dyn/cm. The key effect is a reduction in the range of parameters leading to coexistence of long and short bonds, because the cost of the interface increases.

### Correlation of inner contact area with number of ligands available

The experiments of Grakoui et al. (1999) show a distinct decrease in the size of the center (TCR-pMHC or CD2-CD48) region of the immunological synapse over time. A possible explanation for this phenomenon is that it is caused by down-regulation of TCR over the course of the experiment. In vivo studies suggest that the level of down-regulation can be up to 90% of available TCR (Vallitutti et al., 1996), although this appears to be system-dependent (Itoh et al., 1999).

We use our model to examine the correlation between the number of available TCR and the radius of the inner region of the synapse. Of course, we can only examine the equilibrium state for each case. We present our results in Fig. 7 over a range of possible cell surface tensions. We do find a decrease in the radius of the equilibrium configuration as the number of short receptors (TCR) decreases. We also find that the critical value of the number of short receptors for

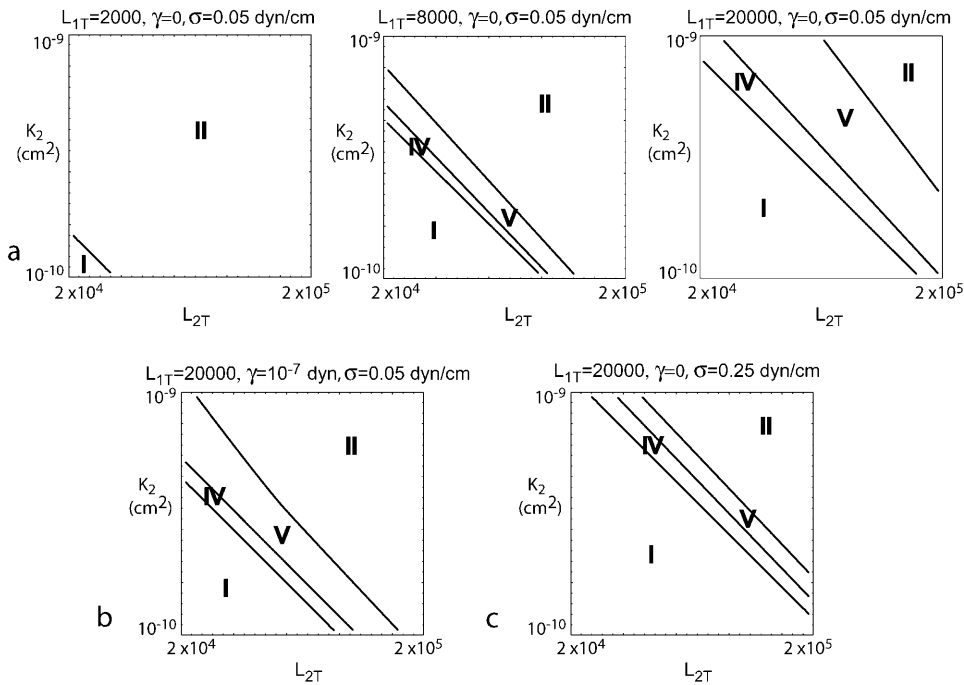


FIGURE 6 Phase diagrams of binding of T cells to antigen-presenting cells highlighting the effects of LFA-1 concentration and binding affinity for ICAM-1.  $L_{1T}$  and  $L_{2T}$  are respectively the numbers of presented pMHC and LFA-1, and  $K_2$  is the equilibrium constant of the LFA-1/ICAM-1 interaction. (a) Comparison of three concentrations of pMHC, with  $\gamma = 0$ . (b) Effect of intercellular repulsion ( $\gamma = 10^{-7}$  dyn). (c) Effect of increasing cellular surface tensions ( $\sigma_{RT} = \sigma_{LT} = 0.25$  dyn/cm). Key: region I, no binding; II, binding solely of ICAM-1/LFA-1 (long bonds); III, binding solely of TCR-pMHC (short bonds); IV, both species bind with TCR-pMHC bonds in the center (immunological synapse); and V, both species bind with ICAM-1/LFA-1 bonds in the center (reversed synapse). Curves have been smoothed.

a transition to a synapse pattern is strongly dependent on the surface tension of the two cells.

### The natural killer cell synapse

An important role of natural killer (NK) cells is to attack cells on which the MHC class I molecule is down-regulated (possibly as a result of viral infection). Similarly to T cells, NK cells form stable attachments to their target cells, where the adhesion is moderated by multiple kinds of ligand-receptor pairs. Again, the long adhesive bonds are formed by ICAM-1/LFA-1 interactions (length 41 nm). A variety of shorter bonds that are important for signaling may also form, of lengths between  $\sim 8$  nm and  $\sim 20$  nm (McCann et al.,

2002). However, there are two important differences between contact regions formed by T cells and NK cells. First, in NK cell synapses, ICAM-1/LFA-1 bonds are found to be stably clustered within the center of the synapse, surrounded by shorter bonds (Davis et al., 1999). Second, the formation of the synapse is unaffected if steps are taken to suppress cytoskeletal effects (specifically, by ATP depletion or use of cytoskeletal inhibitors) (Davis et al., 1999).

As observed above, our model predicts such patterns over a certain range of parameter space. Further, although it is possible that the reversed patterns are a result of kinetic trapping of the long ligand-receptor pairs (which is not addressed by equilibrium modeling), the fact that cytoskeletal inhibition does not alter these “reversed” patterns suggests that a version of our model modified to deal with several ligand-receptor pairs of different lengths might be directly applicable to this system.

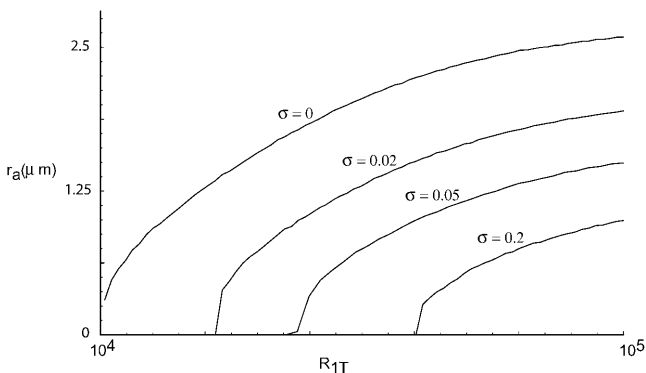


FIGURE 7 Radius of interior region of immunological synapse,  $r_a$ , as a function of available short receptors, for different values of cellular surface tension,  $\sigma_{RT} = \sigma_{LT} = \sigma$ .  $R_{1T}$  is the total number of TCR per cell.

### DISCUSSION

In this article, we have developed a simple, tractable model to describe adhesion between two cells (or a cell and a surface), where that adhesion is mediated by two or more ligand-receptor pairs of varying lengths. Our model relates physical properties of the cells (such as ligand/receptor density, elastic properties of the surface, and properties of the extracellular matrix) and bridging bonds (such as affinity, elasticity, and length) to observables such as segregation of ligand-receptor pairs, size of contact region, and intercellular separation. To achieve the simplicity and generality of the

model, we have followed Bell et al. (1984) in neglecting certain biological properties of cells. We can divide these properties into two classes. First, parameters of the system may well be time-dependent. In particular, the evolution of the parameters may depend on intercellular signaling, which itself is moderated by the success or failure of binding. Second, we have assumed that cells do not actively expend energy to grip each other or push each other away.

Nonetheless, the equilibrium state, governed by well-understood processes of binding and diffusion, can be seen as a null hypothesis, against which more complicated models (including spatial and temporal effects) can be compared. Our theoretical model is directly applicable to possible experimental model systems, where different receptors are held on the surface of lipid vesicles or cells in which cytoskeletal effects are minimized (such as cells treated with cytochalasin). In such systems, our model shows how the nature of adhesion will change as experimental parameters are varied.

As a case study we applied our model to the experimentally well-studied system of the T cell/APC interaction. A problem with modeling this system is the large number of parameters involved, and the level of uncertainty in some of their measurements.

For example, one major question in the analysis of T cell/APC adhesion is whether or not a synapse pattern will form in the absence of directed (cytoskeletal) motion. Experimentally, there is evidence to the contrary for certain systems (Grakoui et al., 1999). The theoretical approach of Burroughs and Wülfing (2002) found that directed motion is required for central aggregation of TCR, whereas the model presented in Lee et al. (2002b) showed synapse formation even in the absence of such a motion. Both groups agree that directed motion is biologically of importance, but the discrepancy between the results of the models indicates that fine details of their construction and of parameter estimation can have large effects. Our model does predict equilibrium synapse formation using similar parameter sets to both previous studies (Figs. 4 and 5), but clearly this result is sensitive to the exact choice of parameters. A major benefit of our approach is that we can very quickly examine wide ranges of possible parameters. Further, our simplified model avoids possible artifacts due to the selection of boundary constraints for a two-dimensional contact area.

A strongly related puzzle is the extent to which a T cell controls adhesion as a function of signals it receives. It has control of the number of cell-surface receptors expressed, the location of those receptors that are cytoskeletally linked, and, for at least one receptor (LFA-1), the affinity with which it binds ligand. The cell shape can also vary quite dramatically. T cell specificity means that the key signals must arrive via the T cell receptor. The signal is therefore potentially controlled by the number of presented pMHC, their affinity for the TCR, the half-life of the pMHC-TCR bond, and (possibly) the spatial distribution of pMHC. Our model cannot address the dynamics of changes, but we can

address questions of how cellular adhesion will vary as the number of receptors or their affinity changes. As an example, we looked at the effects of modifications to LFA-1 number and affinity (Fig. 6). In this vein, a rarely discussed issue that our model can also address is that of cell-cell *unbinding*. For instance, if we suppose an immunological synapse has formed (region IV in Fig. 6) then we can predict whether a change in the number or affinity of LFA-1 would lead to unbinding.

An important consequence of our modeling is that the configuration of a synapse (in the absence of cytoskeletal or other nonequilibrium effects) depends only on the affinity of the TCR-pMHC interaction, and not on the half-life. There has been a debate about which of these parameters is more important in determining the level of T cell activation. Specifically, the kinetic proofreading (McKeithan, 1995) and serial triggering (Valitutti et al., 1995) hypotheses together suggest that there should be a window of half-lives within which cellular activation should be optimal. Experiments have confirmed the existence of this window (Kalergis et al., 2001; Coombs et al., 2002). Recent evidence also shows up the importance of affinity (Holler and Kranz, 2003). The model presented here suggests a middle ground between these two hypotheses: formation of a synapse at equilibrium is dependent on the affinity of the bonds, but the power of cell signaling within the synapse is controlled by kinetic proofreading and serial engagement. Based on Kalergis et al. (2001) and Coombs et al. (2002), it would seem that early nonequilibrium effects (receptor down-regulation and cytoskeletal motion) controlled by successful signaling would be dependent mostly on the half-life.

It is observed that small numbers (10–100) of displayed agonist pMHC are sufficient to lead to synapse formation. Within reasonable parameter ranges, our model does not predict this as an equilibrium state. This suggests that either nonequilibrium processes or effects of other “short” molecules such as CD2 and nonagonist pMHC must play a vital role. If nonequilibrium processes are key, then one or both cells must actively expend energy over the lifetime of the cell-cell contact, not just during its formation. In this light, we draw attention to the natural killer cell synapse. In this system, inhibition of processes requiring energy use (including cytoskeletal motions) does not affect the formation of a “reversed” synapse. This fact suggests that NK cell interactions may be more fit than T cell interactions for study with models invoking only passive properties of cells. Indeed, our model predicts reversed synapse patterns for certain parameter regimes. It is also observed that excess nonagonist pMHC may act to amplify signaling due to small numbers of presented agonists (Wülfing et al., 2002). One can speculate that the nonagonist pMHC are effectively nonspecific short binding molecules and as such make an equilibrium synapse more energetically favorable, but whether such an effect exists will depend on the exact affinities and numbers of such pMHC, and, as always in this

system, on the nature of signaling-induced cell reorientation.

More generally, we can ask how the structure of the immunological synapse and related systems such as the NK cell synapse serve an immunological purpose. T cell activation must be stable and predictable, but there is also a need for T cells to respond quickly to threats. T cell activation might, therefore, be thought of as a threshold switch where signals below a certain level are ignored but the response is strong and immediate above this level. The threshold level might also be adjusted and controlled for each situation. Looking at Figs. 5 and 6, we see phase transitions suggesting a mechanism whereby the signal the TCR receives qualitatively changes (say, from region V to region IV) as the number of pMHC is increased. The exact point of the transition can be controlled by the number of ICAM-1 available (Fig. 5). In fact, if there are too few ICAM-1, then the V–IV transition is impossible. The complexity of the phase diagram increases if we allow the T cell to modulate numbers of TCR and LFA-1, and the affinity of LFA-1, allowing more possibilities for sensitive control of the response to a given stimulus.

## EXPERIMENTAL TESTS

As discussed above, our theory applies to situations where the reorganization of bonds is driven only by thermodynamics. In other words, signaling-induced reorganization must be absent. Second, we require that the cell membrane acts as an essentially passive elastic membrane. Experimentally, the simplest possible system with these properties would consist of an artificial lipid vesicle, with freely diffusing non-interacting receptors of two lengths artificially embedded, interacting with a surface bearing appropriate ligands. Lipid vesicles with a single embedded receptor were studied in the 1980s (Cooper et al., 1981; Balakrishnan et al., 1982a,b). Extending this procedure to have two embedded receptors should be possible.

Experiments revealing immunological synapse formation have been performed with T cells and NK cells (described above). Chemical treatment of cells to block signaling downstream of receptor binding, and with chemical agents to disrupt the cellular cytoskeleton, should lead to an experimental system more amenable to mathematical analysis, at equilibrium or otherwise.

In examining experimental systems, it will be necessary to find one or more defined control parameters to map out the phase space of possible behaviors. In experiments where a cell binds to a supported bilayer, it is possible to vary the density of ligands on the supported bilayer. The natural measurement to take would then be the size of different regions in equilibrated synapse patterns. In bilayer and cell-cell experiments, it would be interesting to try to reproduce the phase plane shown in Fig. 5, by determining the minimum numbers of each ligand/receptor required for

binding, synapse formation, etc. A simpler experiment would be to gradually increase the numbers of short ligands/receptors to see if our prediction that a transition from the normal synapse to the reversed configuration is correct. Manipulation of ligand and receptor densities might be achieved by transfection of ligands or by blocking with monovalent antibodies. In both cell-bilayer and cell-cell experiments the transition to unbinding could be examined by slow addition of blocking agents.

## APPENDIX 1: CALCULATION OF LINE TENSIONS

We need to calculate the line energy due to bending of an interface between short-receptor and long-receptor rich regions of the cell-cell contact area. To do this, we assume that the curvature of the interface in the plane of the contact region is small. In this approximation, the line energy of the interface is just the length of the line times a constant ( $\epsilon_b$ ) with units of energy per length.  $\epsilon_b$  will depend on the change in separation between the membranes, their physical characteristics (surface tensions and bending moduli), and on properties of the forces holding them together (effective spring constants and preferred separations).

We consider two infinite membranes held together by two kinds of ligand-receptor bonds with unstressed lengths  $\zeta_1$ ,  $\zeta_2$ . The membranes are pushed apart by a nonspecific repulsion with potential  $\Gamma$ . The separation is defined to be  $S(x)$ , and the interface is centered at  $x = 0$ . We treat the bonds as linear springs with spring constants  $\kappa_1$ ,  $\kappa_2$  and densities  $b_1$ ,  $b_2$ . The extrinsic force applied to the membrane due to the bonds and the nonspecific repulsion is thus

$$F(S) = -\Gamma'(S) - b_1\kappa_1(S - \zeta_1) - b_2\kappa_2(S - \zeta_2). \quad (22)$$

We now write down the force balance equations (Dembo, 1994) for one membrane, in terms of the membrane position  $(X(a), Y(a))$ , tension  $T(a)$  and curvature  $C(a)$  ( $a$  is arc length along the membrane in the  $x$  direction), and introducing  $\beta$ , the elastic bending modulus of the membrane in question. The force balance in the direction tangent to the membrane is

$$\frac{\partial}{\partial a} \left( T + \frac{1}{2} \beta C^2 \right) = -F(S(x(a)), x(a)) \frac{\partial Y}{\partial a} \quad (23)$$

and in the normal direction,

$$\beta \frac{\partial^2 C}{\partial a^2} - CT = -F(S(x(a)), x(a)) \frac{\partial X}{\partial a}. \quad (24)$$

Making the small angle approximation  $C(s) \simeq C(x) \simeq Y''(x)$  and expanding, we find that, to first order, the surface tension is constant (and therefore equal to its value far from the interface throughout), and we have the following differential equation for  $Y(x)$ :

$$\beta Y''''(x) - TY''(x) = -F(S(x), x). \quad (25)$$

A similar equation applies at the lower membrane (note the sign of the applied force must be reversed). If we let the position of the upper and lower membranes be  $Y_u(x)$  and  $Y_l(x)$ , respectively,  $S(x) = Y_u(x) - Y_l(x)$  and we have a system of two coupled boundary value problems. Note that, in general, the bending moduli and surface tensions of the two cells will not be the same, making the most general solution somewhat involved. Here, we will focus on two special cases, both of practical relevance:

Where the lower membrane is flat and unmoving (to model experiments where a cell contacts a ligand-bearing supported bilayer (Grakoui et al., 1999)).

The symmetric case where the cells have identical bending moduli and surface tension.

## Cell binding to supported bilayer

Let the supported bilayer be at  $y = 0$ , and define the position of the cell membrane to be  $S(x)$ , equal to the membrane separation.  $F(S(x), x)$  changes at  $x = 0$  so we must solve for the left and right solutions of Eq. 25. Each of these will have four constants, two of which are specified by boundary conditions. The remaining four constants are used to match  $S(0)$ ,  $S'(0)$ ,  $S''(0)$ , and  $S'''(0)$ .

Considering the case where the bonds have separated to form a distinct interface around  $x = 0$ , let the bonds have (constant) densities  $b_{1a}, b_{2a}$  for  $x < 0$  and  $b_{1b}, b_{2b}$  for  $x > 0$ . We define

$$F(S, x) = \begin{cases} -\Gamma'(S) - b_{1a}\kappa_1(S - \zeta_1) - b_{2a}\kappa_2(S - \zeta_2) & x < 0 \\ -\Gamma'(S) - b_{1b}\kappa_1(S - \zeta_1) - b_{2b}\kappa_2(S - \zeta_2) & x > 0 \end{cases} \quad (26)$$

We impose that far from the interface, there is no contribution to force balance from intrinsic (elastic) forces:

$$\lim_{x \rightarrow -\infty} F(S(x), x) = 0 \quad (27)$$

$$\lim_{x \rightarrow \infty} F(S(x), x) = 0 \quad (28)$$

and therefore define  $S_a = \lim_{x \rightarrow -\infty} S(x)$  and  $S_b = \lim_{x \rightarrow \infty} S(x)$  by

$$-\Gamma'(S_a) - b_{1a}\kappa_1(S_a - \zeta_1) - b_{2a}\kappa_2(S_a - \zeta_2) = 0 \quad (29)$$

$$-\Gamma'(S_b) - b_{1b}\kappa_1(S_b - \zeta_1) - b_{2b}\kappa_2(S_b - \zeta_2) = 0. \quad (30)$$

As things stand,  $F(S)$  is a nonlinear function of  $S$ . For ease of solution of Eq. 25, we linearize about  $S = S_a$  (for  $x < 0$ ) and  $S = S_b$  (for  $x > 0$ ):

$$F(S, x) \simeq F(S_a) + F'(S_a)(S - S_a) = F'(S_a)(S - S_a) \quad x < 0 \quad (31)$$

$$F(S, x) \simeq F(S_b) + F'(S_b)(S - S_b) = F'(S_b)(S - S_b) \quad x > 0. \quad (32)$$

$$\varepsilon_b = \frac{\beta(S_b - S_a)^2 (\lambda_a \sqrt{\phi_b + 2} + \lambda_b \sqrt{\phi_a + 2})}{4\sqrt{\phi_a + 2}\sqrt{\phi_b + 2}(\lambda_a^4 + \lambda_b^4 + (\lambda_a^3\lambda_b + \lambda_a\lambda_b^3)\sqrt{\phi_a + 2}\sqrt{\phi_b + 2} + \lambda_a^2\lambda_b^2(2 + \phi_a + \phi_b))}. \quad (44)$$

The front will not generally be symmetric about  $x = 0$ . We therefore have two characteristic length scales for the front (from 25).  $\lambda_a = (\beta/F'(S_a))^{1/4}$  is the scale for  $x < 0$  and  $\lambda_b = (\beta/F'(S_b))^{1/4}$  for  $x > 0$ . In both cases,  $F' > 10^7$  ergs/cm<sup>2</sup> (taking the effective spring constant of the most compliant bond to be that of an entropic coil (Doi and Edwards, 1986) and multiplying by an estimate of minimum bond density ( $10^9$  mol/cm<sup>2</sup>)).  $\beta$  is bounded above by  $10^{-13}$ – $10^{-12}$  ergs. We conclude that the boundary layer thickness is  $< 10^{-5}$  cm, small on the micron scale of the whole contact region. We re-scale  $x$  using these scales. Further taking  $s_a = (S - S_a)/S_a$  for  $x < 0$  and  $s_b = (S - S_b)/S_b$  for  $x > 0$ , we have the boundary value problems

$$s_a'''(x) - \phi_a s_a''(x) = -s_a \quad x < 0 \quad (33)$$

$$s_b'''(x) - \phi_b s_b''(x) = -s_b \quad x > 0, \quad (34)$$

where  $\phi_a = T/\sqrt{\beta F'(S_a)}$  and  $\phi_b = T/\sqrt{\beta F'(S_b)}$ . The boundary conditions are that  $s_a(x)$  vanishes as  $x \rightarrow -\infty$  and  $s_b(x)$  vanishes as  $x \rightarrow \infty$ . Solutions satisfying the boundary conditions are

$$s_a(x) = c_1 e^{d_+(\phi_a)x} + c_2 e^{d_-(\phi_a)x} \quad (35)$$

$$s_b(x) = c_1 e^{-d_+(\phi_b)x} + c_2 e^{-d_-(\phi_b)x}, \quad (36)$$

where

$$d_{\pm}(\phi) = \sqrt{\frac{1}{2}(\phi \pm \sqrt{\phi^2 - 4})}. \quad (37)$$

$d_+(\phi)d_-(\phi) = 1$  and  $d_+(\phi) + d_-(\phi) = \sqrt{\phi + 2}$ . The solutions Eqs. 35 and 36 are oscillatory if  $\phi_a < 2$  or  $\phi_b < 2$ . Low tensions, high bending moduli, and high effective spring constants therefore cause oscillatory solutions. Matching the solutions and their first three derivatives at  $x = 0$  gives (abbreviating  $d_{\pm a} = d_{\pm}(\phi_a)$  and  $d_{\pm b} = d_{\pm}(\phi_b)$ ) and returning to dimensional units,

$$S(x) = \begin{cases} S_a + C_1 e^{d_{+a}x/\lambda_a} + C_2 e^{d_{-a}x/\lambda_a} & x < 0 \\ S_b + C_3 e^{-d_{+b}x/\lambda_b} + C_4 e^{-d_{-b}x/\lambda_b} & x > 0 \end{cases} \quad (38)$$

$$C_1 = \frac{(S_b - S_a)\lambda_a^2 d_{-a} d_{-b} d_{+b}}{(d_{-a} - d_{+a})(d_{-b}\lambda_a + d_{+a}\lambda_b)(d_{+a}\lambda_b + d_{+b}\lambda_a)} \quad (39)$$

$$C_2 = \frac{(S_b - S_a)\lambda_a^2 d_{+a} d_{-b} d_{+b}}{(d_{+a} - d_{-a})(d_{-b}\lambda_a + d_{+a}\lambda_b)(d_{+a}\lambda_b + d_{-a}\lambda_b)} \quad (40)$$

$$C_3 = \frac{(S_b - S_a)\lambda_b^2 d_{-a} d_{+a} d_{-b}}{(d_{+b} - d_{-b})(d_{-a}\lambda_b + d_{+b}\lambda_a)(d_{+a}\lambda_b + d_{+b}\lambda_a)} \quad (41)$$

$$C_4 = \frac{(S_b - S_a)\lambda_b^2 d_{-a} d_{+a} d_{+b}}{(d_{-b} - d_{+b})(d_{-a}\lambda_b + d_{+b}\lambda_a)(d_{-b}\lambda_a + d_{+a}\lambda_b)}. \quad (42)$$

The energy of such an interface is

$$\varepsilon_b = \int_{-\infty}^{\infty} \frac{\beta}{2} C(a)^2 da \simeq \int_{-\infty}^{\infty} \frac{\beta}{2} S''(x)^2 dx. \quad (43)$$

Using the solution Eq. 38, we find

## Two cells in contact—symmetrical case

We now look at the case where two cells with identical membrane bending modulus ( $\beta$ ) and surface tension ( $T$ ) are in contact. From Eq. 25, we have coupled equations for the (upper and lower) membrane positions  $Y_u$  and  $Y_l$ :

$$\beta Y_u'''' - T Y_u'' = -F(Y_u - Y_l, x) \quad (45)$$

$$\beta Y_l'''' - T Y_l'' = F(Y_u - Y_l, x). \quad (46)$$

Subtracting Eq. 45 from Eq. 46, we have a single equation for the membrane separation

$$\beta S'''' - T S'' = -2F(S, x). \quad (47)$$

The method of solution is identical to the previous case. In the end, the bending energy associated with a transition from long to short bonds is given by

$$\varepsilon_b = \int_{-\infty}^{\infty} \frac{\beta}{2} (Y_u''(x)^2 + Y_l''(x)^2) dx = \int_{-\infty}^{\infty} \frac{\beta}{4} S''(x)^2 dx. \quad (48)$$

$S$  is given by Eq. 38, but replacing  $F'$  with  $2F'$  in the definitions of  $\lambda_a$ ,  $\lambda_b$ ,  $\phi_a$ , and  $\phi_b$ . Using typical parameters (Table 2), the energy density is found to be on the order of  $10^4 - 10^5 k_B T/cm$ , corresponding to  $\sim 10 k_B T$  for an interface of length a few microns.

## APPENDIX 2: PARAMETER ESTIMATES FOR THE T CELL SYSTEM

### T cell receptor interaction

The basic situation we consider is that of a T cell bearing  $3 \times 10^4$  identical TCR (Shaw and Dustin, 1997), interacting with an APC bearing 100–1000 agonist peptides. Two-dimensional affinities for this interaction are in the range of  $4 \times 10^{-11} - 1 \times 10^{-9} \text{ cm}^2$  (Wofsy et al., 2001). This bond is taken to have an unstrained length of 14 nm (Wild et al., 1999).

### LFA-1/ICAM-1 interaction

We suppose the T cell bears  $3 \times 10^5$  LFA-1 molecules (Lollo et al., 1993). We take the concentration of ICAM-1 on the APC to be the same as in the experiments of Grakoui et al. (1999),  $200 \text{ mol}/\mu\text{m}^2$ . This bond has an unstrained length of 41 nm (Wild et al., 1999) and, as described above, the affinity varies. On unstimulated T cells, the affinity has been measured to be  $K = 10^4 \text{ M}^{-1}$  (Lollo et al., 1993), corresponding to a two-dimensional affinity  $K_2 = 1.7 \times 10^{-11} \text{ cm}^2$ . On stimulation of the T cells, this affinity increases by a factor of 200–300.

### Mechanical properties

The bond elasticities are assumed to be the same and are on the order of 0.1 dyn/cm (Bell et al., 1984). We assume the two cells are otherwise identical, and are characterized by resting surface areas of  $5 \times 10^{-6} \text{ cm}^2$ , bending moduli  $\sim 5 \times 10^{-13} \text{ erg}$  (Raucher et al., 2000) and surface tensions  $\sim 0.1 \text{ dyn/cm}$  (as measured for a neutrophil by Needham and Hochmuth, 1992). The intercellular repulsion is characterized by two parameters, a force scale  $\gamma = 10^{-6} \text{ dyn}$  and a length scale  $\tau = 10^{-6} \text{ cm}$  (Bell et al., 1984).

This work was supported by National Institutes of Health grant R37-GM35556 and performed under the auspices of the U.S. Department of Energy.

## REFERENCES

- Balakrishnan, K., F. J. Hsu, A. D. Cooper, and H. M. McConnell. 1982a. Lipid hapten containing membrane targets can trigger specific immunoglobulin E-dependent degranulation of rat basophil leukemia cells. *J. Biol. Chem.* 257:6427–6433.
- Balakrishnan, K., S. Q. Mehdi, and H. M. McConnell. 1982b. Availability of dinitrophenylated lipid haptens for specific antibody binding depends on the physical properties of host bilayer membranes. *J. Biol. Chem.* 257:6434–6439.
- Bell, G. I., M. Dembo, and P. Bongrand. 1984. Cell adhesion. Competition between nonspecific repulsion and specific bonding. *Biophys. J.* 45:1051–1064.
- Bell, G. I., and D. C. Torney. 1985. On the adhesion of vesicles by cell adhesion molecules. *Biophys. J.* 48:939–947.
- Bongrand, P., and G. I. Bell. 1984. Cell-cell adhesion: Parameters and possible mechanisms. In *Cell Surface Dynamics: Concepts and Models*. C. Delisi, A. S. Perelson, and F. Wiegand, editors. Marcel Dekker, New York. 459–493.
- Burridge, K., and M. Chrzanowska-Wodnicka. 1996. Focal adhesions, contractility, and signaling. *Annu. Rev. Cell Dev. Biol.* 12:463–518.
- Burroughs, N. J., and C. Wülfing. 2002. Differential segregation in the cell:cell contact interface—the dynamics of the immunological synapse. *Biophys. J.* 83:1784–1796.
- Coombs, D., A. M. Kalergis, S. G. Nathenson, C. Wofsy, and B. Goldstein. 2002. Activated TCRs remain marked for internalization after dissociation from peptide-MHC. *Nat. Immunol.* 3:926–931.
- Cooper, A. D., K. Balakrishnan, and H. M. McConnell. 1981. Mobile haptens in liposomes stimulate serotonin release by rat basophilic leukemia cells in the presence of specific immunoglobulin E. *J. Biol. Chem.* 256:9379–9381.
- Davis, D. M., I. Chiu, M. Fassett, G. B. Cohen, O. Mandelboim, and J. L. Strominger. 1999. The human natural killer cell immune synapse. *Proc. Natl. Acad. Sci. USA.* 96:15062–15067.
- Davis, S. J., and P. A. van der Merwe. 1996. The structure and ligand interactions of CD2: implications for T-cell function. *Immunol. Today.* 17:177–187.
- Delon, J., S. Stoll, and R. N. Germain. 2002. Imaging of T-cell interactions with antigen presenting cells in culture and in intact lymphoid tissue. *Immunol. Rev.* 189:51–63.
- Dembo, M. 1994. On peeling an adherent cell from a surface. *Lectures on Mathematics in the Life Sciences.* 24:51–77.
- Dembo, M., and G. I. Bell. 1987. The thermodynamics of cell adhesion. *Curr. Topics Memb. Trans.* 29:71–89.
- Doi, M., and S. F. Edwards. 1986. *The Theory of Polymer Dynamics*. Clarendon Press, Oxford.
- Dustin, M. L., D. E. Golan, D.-M. Zhu, J. M. Miller, W. Meier, E. A. Davies, and P. A. van der Merwe. 1997. Low affinity interaction of human or rat T cell adhesion molecule CD2 with its ligand aligns adhering membranes to achieve high physiological affinity. *J. Biol. Chem.* 272:30889–30898.
- Dustin, M. L., M. W. Olszowy, A. D. Holdorf, J. Li, S. Bromley, N. Desai, P. Widder, F. Rosenberger, P. A. van der Merwe, P. M. Allen, and A. S. Shaw. 1998. A novel adapter protein orchestrates receptor patterning and cytoskeletal polarity in T-cell contacts. *Cell.* 94:667–677.
- Dustin, M. L., and A. S. Shaw. 1999. Costimulation: building an immunological synapse. *Science.* 283:649–650.
- Forscher, P., C. H. Lin, and C. Thompson. 1992. Novel form of growth cone motility involving site directed actin filament assembly. *Nature.* 357:515–518.
- Freiberg, B. A., H. Kupfer, W. Maslanik, J. Delli, J. Kappler, D. M. Zaller, and A. Kupfer. 2002. Staging and resetting T cell activation in SMACs. *Nat. Immunol.* 3:911–917.
- Grakoui, A., S. K. Bromley, C. Sumen, M. M. Davis, A. S. Shaw, P. M. Allen, and M. L. Dustin. 1999. The immunological synapse: a molecular machine controlling T cell activation. *Science.* 285:221–227.
- Hogg, N., R. Henderson, B. Leitinger, A. McDowall, J. Porter, and P. Stanley. 2002. Mechanisms contributing to the activity of integrins on leukocytes. *Immunol. Rev.* 186:164–171.
- Holler, P. D., and D. M. Kranz. 2003. Quantitative analysis of the contribution of TCR/pepMHC affinity and CD8 to T cell activation. *Immunity.* 18:255–264.
- Hori, Y., S. Raychaudhuri, and A. K. Chakraborty. 2002. Analysis of pattern formation and phase segregation in the immunological synapse. *J. Chem. Phys.* 117:9491–9501.
- Huang, J.-F., Y. Yang, H. Sepulveda, W. Shi, I. Hwang, P. Peterson, M. R. Jackson, J. Sprent, and Z. Cai. 1999. TCR-mediated internalization of peptide-MHC complexes acquired by T cells. *Science.* 286:952–954.
- Itoh, Y., B. Hemmer, R. Martin, and R. N. Germain. 1999. Serial TCR engagement and down-modulation by peptide:MHC molecule ligands: relationship to the quality of individual TCR signaling events. *J. Immunol.* 162:2073–2080.
- Jockusch, B. M., P. Bubeck, K. Giehl, M. Kroemker, J. Moschner, M. Rothkegel, M. Rudiger, K. Schluter, G. Stanke, and J. Winkler. 1995. The molecular architecture of focal adhesions. *Annu. Rev. Cell Dev. Biol.* 11:379–416.

- Johnson, K. G., S. K. Bromley, M. L. Dustin, and M. L. Thomas. 2000. A supramolecular basis for CD45 tyrosine phosphatase regulation in sustained T cell activation. *Proc. Natl. Acad. Sci. USA*. 97:10138–10143.
- Kalergis, A. M., N. Boucheron, M.-A. Doucey, E. Palmieri, E. C. Goyarts, Z. Vegh, I. G. Luescher, and S. G. Nathenson. 2001. Efficient T cell activation requires an optimal dwell-time of interaction between the TCR and the pMHC complex. *Nat. Immunol.* 2:229–234.
- Krummel, M. F., and M. M. Davis. 2002. Dynamics of the immunological synapse: finding, establishing and solidifying a connection. *Curr. Opin. Immunol.* 14:66–74.
- Kupfer, A., T. R. Mosmann, and H. Kupfer. 1991. Polarized expression of cytokines in cell conjugates of helper T cells and splenic B cells. *Proc. Natl. Acad. Sci. USA*. 88:775–779.
- Kupfer, H., C. R. F. Monks, and A. Kupfer. 1994. Small splenic B cells that bind to antigen-specific T helper (Th) cells and face the site of cytokine production in the Th cells selectively proliferate: immunofluorescence microscopic studies of Th-B antigen-presenting cell interactions. *J. Exp. Med.* 179:1507–1515.
- Lee, K. H., A. D. Holdorf, M. L. Dustin, A. C. Chan, P. M. Allen, and A. S. Shaw. 2002a. T cell receptor signaling precedes immunological synapse formation. *Science*. 295:1539–1542.
- Lee, S.-J. E., Y. Hori, J. T. Groves, M. L. Dustin, and A. K. Chakraborty. 2002b. Correlation of a dynamic model for immunological synapse formation with effector functions: two pathways to synapse formation. *Trends Immunol.* 23:492–499.
- Lee, S.-J. E., Y. Hori, J. T. Groves, M. L. Dustin, and A. K. Chakraborty. 2002c. The synapse assembly model. *Trends Immunol.* 23:500–502.
- Liu, H., M. Rhodes, D. L. Wiest, and D. A. A. Vignali. 2000. On the dynamics of TCR:CD3 complex cell surface expression and down modulation. *Immunity*. 13:665–675.
- Lollo, B. A., K. W. H. Chan, E. M. Hanson, V. T. Moy, and A. A. Brian. 1993. Direct evidence for two affinity states for lymphocyte function-associated antigen 1 on activated T cells. *J. Biol. Chem.* 268:21693–21700.
- McCann, F. E., K. Suhling, L. M. Carlin, K. Eleme, S. B. Taner, K. Yanagi, B. Vanherbergen, P. M. W. French, and D. M. Davis. 2002. Imaging immune surveillance by T cells and NK cells. *Immunol. Rev.* 189:179–192.
- McKeithan, K. 1995. Kinetic proofreading in T-cell receptor signal transduction. *Proc. Natl. Acad. Sci. USA*. 92:5042–5046.
- Monks, C. R., B. A. Freiberg, H. Kupfer, N. Sciaky, and A. Kupfer. 1998. Three-dimensional segregation of supramolecular activation cluster in T cells. *Nature*. 395:82–86.
- Moss, W. C., D. J. Irvine, M. M. Davis, and M. F. Krummel. 2002. Quantifying signaling-induced reorientation of T cell receptors during immunological synapse formation. *Proc. Natl. Acad. Sci. USA*. 99:15024–15029.
- Needham, D., and R. Hochmuth. 1992. A sensitive measure of surface stress in the resting neutrophil. *Biophys. J.* 61:1664–1670.
- Press, W. H., B. P. Flannery, S. A. Teukolsky, and W. T. Vetterling. 1988. *Numerical Recipes in C*. Cambridge University Press, New York.
- Qi, S. Y., J. T. Groves, and A. K. Chakraborty. 2001. Synaptic pattern formation during cellular recognition. *Proc. Natl. Acad. Sci. USA*. 98:6548–6553.
- Raucher, D., T. Stauffer, W. Chen, K. Shen, S. Guo, J. York, M. Sheetz, and T. Meyer. 2000. Phosphatidylinositol 4,5-bisphosphate functions as a second messenger that regulates cytoskeleton-plasma membrane adhesion. *Cell*. 100:221–228.
- Schmid-Schönbein, G. W., Y. Y. Shih, and S. Chien. 1980. Morphometry of human leukocytes. *Blood*. 56:866–875.
- Shaw, A. S., and M. L. Dustin. 1997. Making the T cell receptor go the distance: a topological view of T cell activation. *Immunity*. 6:361–369.
- Stewart, M., and N. Hogg. 1996. Regulation of leukocyte integrin function: affinity vs. avidity. *J. Cell. Biochem.* 61:554–561.
- Ting-Beall, H. P., D. Needham, and R. Hochmuth. 1993. Volume and osmotic properties of neutrophils. *Blood*. 81:2774–2780.
- Torney, D. C., M. Dembo, and G. I. Bell. 1986. Thermodynamics of cell adhesion, II. Freely mobile repellers. *Biophys. J.* 49:501–507.
- Valitutti, S., M. Dessing, K. Aktories, H. Gallati, and A. Lanzavecchia. 1995. Sustained signaling leading to T cell activation results from prolonged T cell receptor occupancy. Role of T cell actin cytoskeleton. *J. Exp. Med.* 181:577–584.
- Vallitutti, S., S. Müller, M. Cella, E. Padovan, and A. Lanzavecchia. 1996. Serial triggering of many T-cell receptors by a few pMHC complexes. *Nature*. 375:148–151.
- van der Merwe, P. A. 2002. Formation and function of the immunological synapse. *Curr. Opin. Immunol.* 14:293–298.
- van der Merwe, P. A., and S. J. Davis. 2002. The immunological synapse: a multitasking system. *Science*. 295:1479–1480.
- Weikl, T. R., J. T. Groves, and R. Lipowsky. 2002. Pattern formation during adhesion of multicomponent membranes. *Europhys. Lett.* 59:916–922.
- Wild, M. K., A. Cambiaggi, M. H. Brown, E. A. Davies, H. Ohno, T. Saito, and P. A. van der Merwe. 1999. Dependence of T cell antigen recognition on the dimensions of an accessory receptor-ligand complex. *J. Exp. Med.* 190:31–41.
- Wofsy, C., D. Coombs, and B. Goldstein. 2001. Calculations show substantial serial engagement of T cell receptors. *Biophys. J.* 80:606–612.
- Wülfing, C., and M. M. Davis. 1998. A receptor/cytoskeletal movement triggered by costimulation during T cell activation. *Science*. 282:2266–2269.
- Wülfing, C., C. Sumen, M. D. Sjaastad, L. C. Wu, M. L. Dustin, and M. M. Davis. 2002. Costimulation and endogenous MHC ligands contribute to T cell recognition. *Nat. Immunol.* 3:42–47.
- Žal, T., M. A. Žal, and N. R. J. Gascoigne. 2002. Inhibition of T cell receptor-coreceptor interactions by antagonist ligands visualized by live FRET imaging of the T-hybridoma immunological synapse. *Immunity*. 16:521–534.